Experimental transients of detonation re-initiation behind a single-hole obstacle: the effects of the tube cross-section shape

Vianney Monnier, V. Rodriguez, Léa Vilasi, Pierre Vidal, Ratiba Zitoun

Experimental transients of detonation re-initiation behind a single-hole obstacle: the effects of the tube cross-section shape

Vianney Monnier*, Vincent Rodriguez, Léa Vilasi, Pierre Vidal, Ratiba Zitoun

Institut Pprime, UPR 3346 CNRS, ISAE-ENSMA, Futuroscope-Chasseneuil, 86961, France

*Corresponding author: vianney.monnier@laas.fr

March 28, 2025.

Abstract

We describe the scenarios of detonation re-initiation downstream of a single-hole obstacle in a straight tube depending on its cross-sectional shape, namely square or round. The tubes have the same cross-sectional area of 16 cm^2, and the holes have the same shape as that of the tubes, but different open area ratios. The reactive mixtures are $2\,H_2 + O_2 + 2\,Ar$ and $2\,H_2 + O_2$. We used wall soot recordings, high-speed shadowgraphy or chemiluminescence imaging to obtain parietal and frontal views of the diffraction phenomena. We identify six behaviors, one subcritical, four critical, and one supercritical, depending on the initial pressure. The critical and supercritical behaviors are more easily obtained in the square tube than in the round tube, other parameters being equal. These transient effects of the cross-sectional shape can be observed where no effect would be observed for conditions of steady propagation. Inductively, this leads to discuss what dimensionality refers to experimentally for the global and local transients of detonation dynamics.

[1]

1 Introduction

Detonation diffraction is an important topic in detonation dynamics because of its applications in industrial safety or the design of initiation devices in aerospace equipment, *e.g.*, the chamber of rotating engines. A large number of studies [1] have addressed detonation diffraction for various configurations, in particular the shape of the obstacle, the number or shape of holes in the obstacle [2], but to our knowledge not the effect of the cross-sectional shape of the tube. In this article we detail our experimental investigation [3, 4] on the diffraction scenarios of a steady cellular detonation from a single-hole obstacle depending on the cross-sectional shape of the tube, namely square or round. In fact, the square channels are convenient for visualization in the laboratory, but the round tubes are the rule in industry, both for practical and economic reasons.

Studies on detonation diffraction usually describe up to two critical scenarios, *e.g.* [5, 6] or are limited to two dimensions [7, 8]. Successful detonation propagation in premixed reactive media requires the coupling of the combustion wave with its preceding shock wave [9, 10]. Their decoupling unbalances the energy production and loss and can lead to the quenching of the self-sustained detonation [11, 12]. Such decoupling occurs when the detonation diffracts during its transmission to confinements of greater dimensions [13, 14, 15, 16, 6].

[1] Article submitted to Shock Waves Journal

The study on the latter by Zeldovich et al. is the one that introduced the notions of sub- and super-critical behaviors in detonation transient dynamics [17]. Subcritical behavior refers to detonation extinction with no re-initiation, that is, the disappearance of the cellular structure. Critical behaviors are cases of detonation quenching followed by re-initiation, that is, cellular structure discontinuity. For critical behaviors, detonation re-ignition phenomena in a tube generally result from hot spots. These heterogeneities can have several origins, possibly combined, such as wall defects, turbulent boundary layers, or non-uniform initial states (pressure, temperature gradients) from which a self-accelerating flame is born [18]. Compression waves propagate upstream of the flame front, inducing a self-amplification process until a shock wave forms. This shock wave can become strong-enough to initiate an explosion in the mixture between the shock and the flame. Detonation then occurs if the shock-combustion coupling conditions are maintained. This canonical mechanism is called SWACER (Shock Wave Amplification by Coherent Energy Release) [19, 20]. Supercritical behaviors are continuous propagation of the detonation, whether its velocity, cell size or regularity vary or not. Local extinction may occur, typically in the vicinity of the giver section exit.

The mean width $\bar{\lambda}$ measured on parietal recordings is still considered a characteristic length. This length is convenient for detonation dynamics analysis, in particular, to predict the detonation behavior during transient phenomena [21]. Studies following the one by Zeldovich et al. lead to criteria for the successful transmission of detonation (that is, critical to supercritical behaviors) based on cell-to-tube widths ratio, with the critical diameter of the giver section $d_c \simeq 10$ to $30\bar{\lambda}$ [22], depending on the cellular structure regularity [23, 24, 25], mixture initial temperature [26], or if the channel is 2D or 3D [27]. That criterion is used for presizing detonation arresters, but other parameters exist, such as obstacle shapes, spacings, open area ratios, number of holes, sizes, *etc* [28]. If the obstacle is several cell lengths thick, it behaves as a confinement reduction, and if its open area transverse dimension is lower than the critical dimension for propagation, equivalently the cell mean width, the detonation quenches within the obstacle. If the shock wave does not decouple with the combustion wave within the obstacle, the change of open area diffracts the detonation.

The confinement cross-section shape and area (A) influence the propagation of a self-sustained detonation in a straight channel [29]. This influence manifests itself by a difference in the detonation cell mean width $\bar{\lambda}$ from one confinement geometry to another, all initial thermodynamical (initial pressure p_0 and temperature T_0) and chemical (composition, Equivalence Ratio ER) conditions of the reactive mixture being equal. However, if the parameters (A, p_0) are sufficiently large [29, 30], the geometry no longer affects $\bar{\lambda}$, and the front-view soot recordings of the detonation show irregular patterns. This results in a large number ($\mathcal{O}(100)$) of cells per unit area on the detonation front. In this situation, the cells can be termed as self-confined [3], being independent on the transverse dimension and the cross-sectional shape of the tube.

Section 2 presents the experimental setup and methodology. Section 3 details the results from the diffraction and the re-ignition of the detonation passing through a single-hole obstacle for two shapes of tubes. Section 4 discusses the results and proposes some conclusions.

2 Experimental setup and methodology

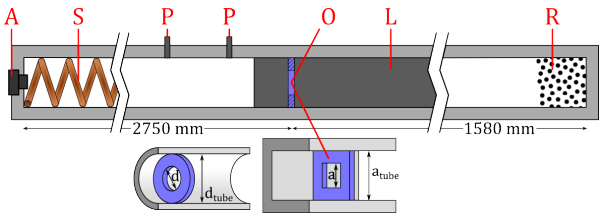

Fig. 1: Square tube (or round) with 16 cm^2 cross section area. A: ignition, S: Shchelkin spiral, P: piezo-electric pressure gauges, O: obstacle, L: soot-coated surface or quartz windows, R: steel wood

We performed our experiments with two similar tubes with a round or square cross sections of the same area of 16±4% cm^2. Figure 1 shows a schematic of the round or square tube. Either a spark plug or an exploding wire (Fig. 1, A) ignited the combustion of the reactive mixture. A Shchelkin spiral (Fig. 1, S) promoted transition to detonation

within 1 meter from ignition. The obstacle (Fig. 1, O) consisted of a 5 mm-thick plate perforated with a single hole of the same shape as the straight channel cross-section, *i.e.*, a square hole in the square channel and a round hole in the round tube. It was placed 2750 mm away from ignition. In this study, the Opening Area Ratio (OAR) is the ratio of the cross-sectional area of the orifice to the cross-sectional area of the tube, which varies from OAR= 10 to 75%. A steel wool ball (Fig. 1, R) dampened the shock wave before it reflected off the bottom flange at the end of the wall.

We recorded pressure signals upstream of obstacles with Kistler 603B piezoelectric pressure transducers (Fig. 1, P) coupled to Kistler 5018A electrostatic charge amplifiers whose triggering times indicated both the detonation steadiness and its average velocity. Parietal soot foils (Fig. 1, L) recorded the cellular structures of the detonation upstream and downstream of the obstacle. In the square channel, quartz windows could replace those soot-coated surfaces to enable high-speed shadowgraph (Fig. 2) or chemiluminescence recordings.

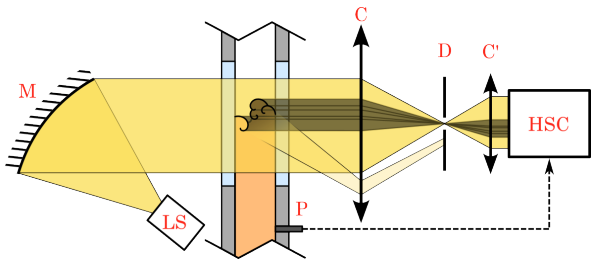

Fig. 2: Shadowgraph setup of the square tube for this study. LS: Light Source, M: Mirror, C: Converging lens, D: Diaphragm, C': Collection lens, HSC: Shimazu HPVX-2 High Speed Camera, P: Piezoeletric transducer (the signal amplifier is not represented for clarity). Dotted arrow: triggering information.

For chemiluminescence imaging, a Shimadzu HPVX-2 camera recorded 256 images of emitted light from the burnt gases with an opening time of 200 ns and a frequency set from 0.5 to 2 MHz. The camera started recording the images after a delay from the triggering time of the closest upstream pressure transducer and amplifier (Fig. 2, P). The delay time was set according to detonation velocities measured in previous experiments [29] and compiled in Fig. 3. For shadowgraph imaging, a 500 watts mercury vapor lamp (Fig. 2, SL) emitted a conical light beam towards a concave mirror (Fig. 2, M) of 1.5 m focal length and ∅150 mm diameter. The converging lens and collecting lens (Fig. 2, C and C') had 750 and 65 mm focal lengths, ∅150 and ∅50 mm diameters, respectively. The diaphragm had a ∅1 mm round opening.

The shadograph and chemiluminescence techniques show integrated information across the camera depths of field, hence require front-view recordings to fully appreciate the three-dimensional aspects of the wave dynamics, that is, differentiate information in the width of the tube. In both the round and square channels, removing the damping steel wool (R) and replacing the end flange with a quartz window enabled front-view chemiluminescence recordings downstream of the obstacle.

We selected the stoichiometric reactive mixtures $2\,H_2 + O_2$ and $2\,H_2 + O_2 + 2\,Ar$. The mixture was prepared in a separate tank using the partial-pressure method and then injected at the initial pressure p_0 after vacuuming the tubes at $T_0 = 294 \pm 3$ K.

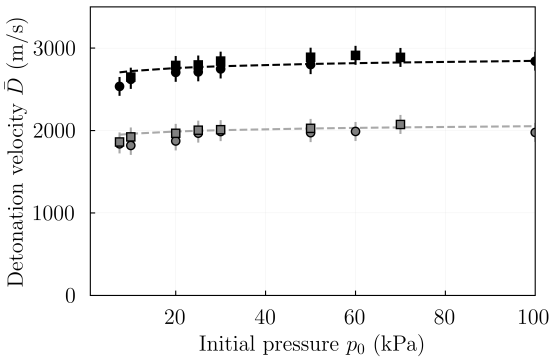

Fig. 3: Average detonation velocities $\bar{D}$ in square (□) and round (○) 16cm² tubes as a function of initial pressure p_0, and Argon dilution [3]. Dotted lines are Chapman-Jouguet velocities. Experimental uncertainties evaluated by [31] are 115 m/s.

3 Experimental results

The experiments showed very high repeatability, thus allowing superposition of results from soot recordings, shadowgraph and chemiluminescence imaging, as in Figure 4.

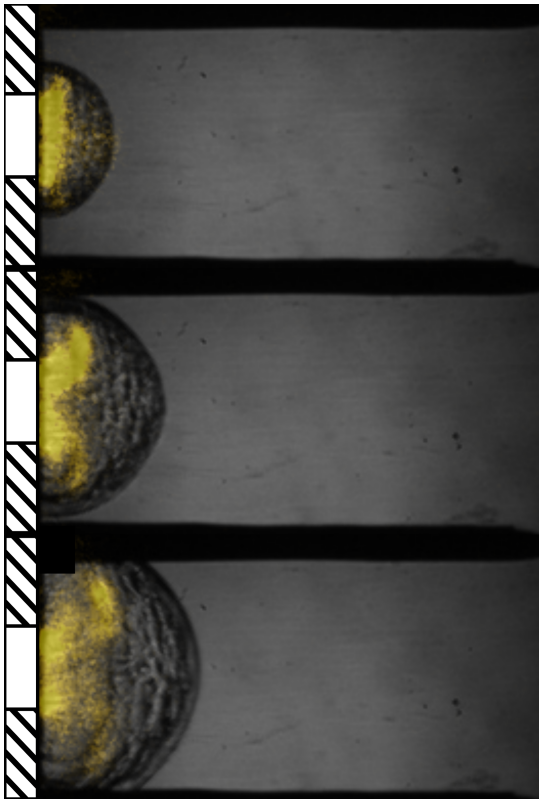

Fig. 4: Shock wave diffraction and decoupling of the combustion wave after passing through the obstacle with OAR=10% (square cross section tube). The mixture is $2\,H_2 + O_2$ at $p_0 = 60$ kPa (superposition of colorized chemiluminescence and shadowgraph images, camera frequency: 250 kHz).

We have identified six diffraction scenarios. One is subcritical, four are critical, one is supercritical. For each mixture, the parameters (OAR, p_0) determine the occurrence of a scenario. The common feature of each scenario is that the shock generated by diffraction through the obstacle interacts symmetrically with the tube wall(s). Analysis of the recordings shows that this interaction generates four Mach waves in the square tube and one toroidal Mach wave in the round tube. Each wave propagates along the wall(s) and converges towards the tube axis. The scenarios differ in whether and how the reflected wave participates in the re-initiation of the detonation. These scenarios are:

- No re-initiation of the detonation downstream of the obstacle (Subsec. 3.1). This subcritical scenario occurs at low OAR or p_0.
- Re-initiation of detonation by the convergence of shocks in the centerline of the tube, only observed in the square tube (Subsec. 3.2).
- Re-initiation of detonation by convergence of shocks in section corners, only observed in the square tube (Subsec. 3.2).
- Re-initiation of detonation by Deflagration-to-Detonation Transition (Subsec. 3.3). This critical scenario occurs at low OARs (OAR$\leq$ 25% in round tube and OAR= 10% in square tube).
- Re-initiation of detonation by shock reflection on the wall (Subsec. 3.3). This critical scenario occurs at high initial pressures or intermediate OARs.
- Supercritical transmission of detonation without extinction (Subsec. 3.4). This scenario occurs for OAR$\geq$ 50% for the round tube and OAR= 75% for the square tube.

Shadowgraph and chemiluminescence imaging (figure 4) and soot recordings provide an overview of the diffraction dynamics over the entire cross section in the square tube, and the soot recordings provide information about the cell structure on the walls of both the round and square tubes.

3.1 Detonation Diffraction, Quenching, and Subcritical Scenario

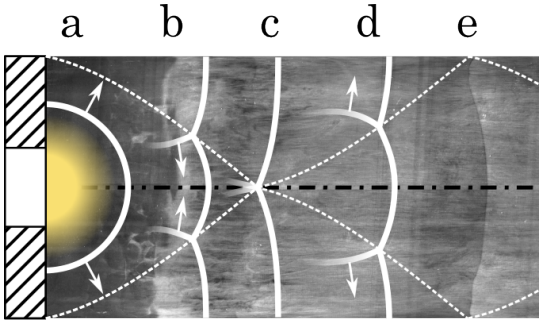

Fig. 5: Schematic of the diffraction process downstream of the obstacle in the round tube.

Figure 5 shows a schematic of the axisymmetric diffraction process over a soot recording, and figure 6 shows shadowgraph images with the corresponding soot recording from the square tube. When the shock wave diffracts, the detonation loses strength as the expansion wave moves toward

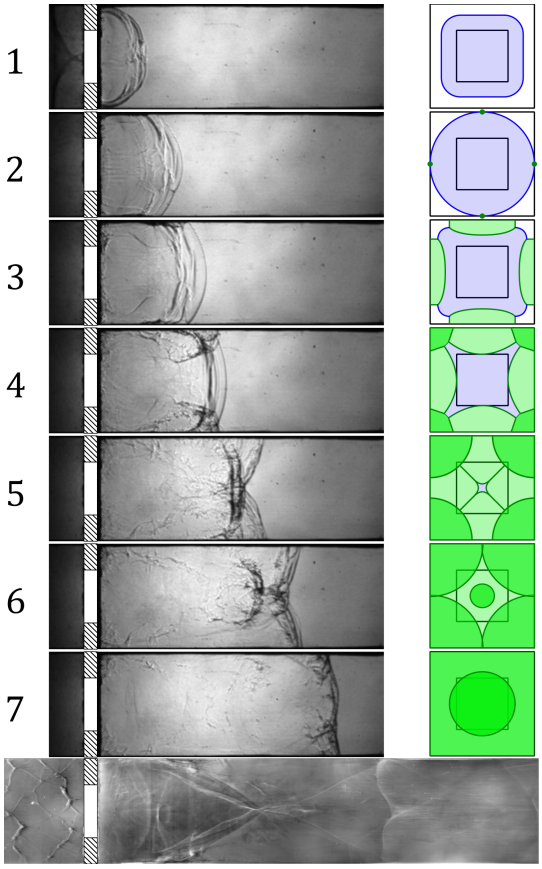

Fig. 6: Diffraction with OAR=25%. The mixture is $2\,H_2 + O_2$ at $p_0 = 15$ kPa. Shadowgraph images (1 to 7, left: longitudinal recordings), parietal soot recording (bottom), front view schemes (right). $\Delta t_{\text{images}} = 6,5$ μs. Tube cross-section: $40{\times}40$ mm^2.

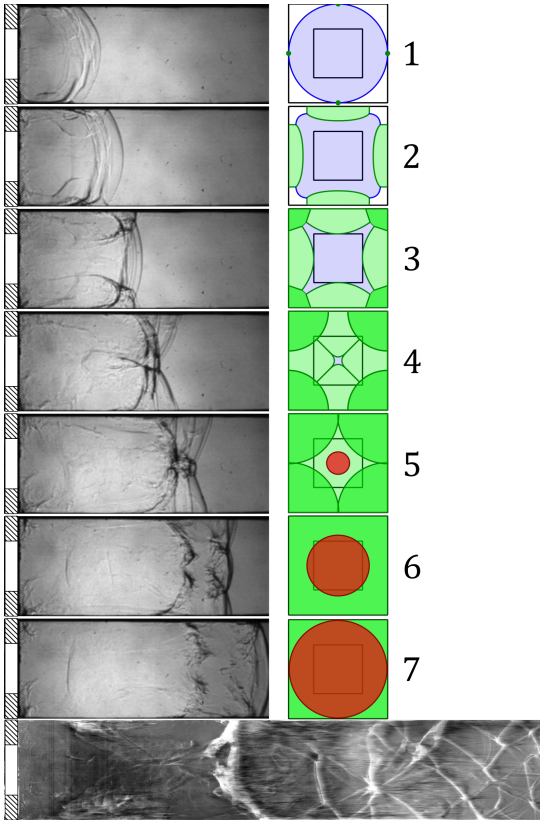

Fig. 7: Diffraction with OAR=25%. The mixture is $2\,H_2 + O_2 + 2\,Ar$ at $p_0 = 12.5$ kPa. Shadowgraph images (1 to 7, left: longitudinal recordings), parietal soot recordings (bottom), front view schemes (right). $\Delta t_{\text{images}} = 8,5$ μs.

the center of the tube. This reduction in strength causes the temperature downstream of the shock to drop, increasing the induction time [32]. The reaction zone eventually decouples from the shock [33, 34, 11, 35] and the detonation quenches (Fig. 5, a and Fig. 6, 1). The diffracted shock wave then reflects on the tube wall(s). In the round tube, the diffracted shock reflects on the circle defined as the intersection between the obstacle and the tube wall, reflecting a toroidal shock wave sweeping along the tube wall and towards the tube axis of symmetry (Fig. 5, b). In the square tube, the diffracted shock reaches the four tube walls closest to the orifice, *i.e.*, the points located in the center of the walls (Fig. 6, 2), resulting in four reflected shocks propagating towards the centerline of the tube and along the walls of the tube (Fig. 6, 3). Those shock waves then combine by pairs at the corners of the tube (Fig. 6, 4-5). In both round and square channels, the reflected shock(s) refocus at the center of the tube to form a recombined shock kernel (Fig. 5, c and Fig. 6, 6) that propagates outwards to the tube wall(s) to imprint on the sooted surface 5, d-e and Fig. 6, 7). The previous steps periodically start again until the shocks fade or reflect on the end wall. In the phenomena described above, there is no re-initiation of the detonation downstream of the obstacle, that is, this scenario is subcritical. Removing the damping wool (Fig. 1, R) may result in re-initiations when the inert shock reflects on the end wall, as in [36, 37, 38], for high enough initial pressures. Those cases are not within the scope of the present study.

3.2 Shock-shock Interactions Critical Scenarios

Figure 7 shows the case of a detonation in $2\,H_2 + O_2 + 2\,Ar$ at $p_0 = 12.5$ kPa diffracted by the obstacle with OAR = 25% in the square tube. The waves reflected from the walls converge toward the tube axis. Their convergence produces a wave strong enough to ignite the mixture and re-initiate a diverging detonation (Fig. 7, 5-6) that propagates partly in the pre-shocked medium, where fresh and burnt gases are present, and partly in the fresh mixture. This divergent detonation reaches the walls after expansion and becomes flat again. Soot recordings (Fig. 7) show a parietal cellular structure that is more irregular downstream of the obstacle than upstream. This irregularity is due to the presence of burnt gases along with fresh mixture. As the re-initiated detonation propagates, it stabilizes in fresh mixture.

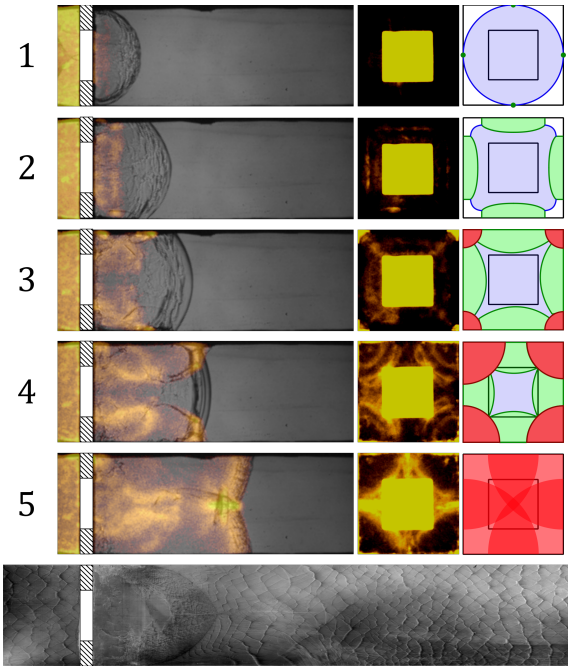

Fig. 8: Diffraction with OAR=25%. The mixture is $2\,H_2 + O_2$ at $p_0 = 30$ kPa. Superposition of colorized chemiluminescence and shadowgraph images (1 to 5, left: longitudinal recordings), chemiluminescence front recordings (middle), soot recording (bottom), and front views schemes (right). $\Delta t_{\text{images}} = 3$ μs.

Figure 8 shows the case of a detonation of $2\,H_2 + O_2$ at $p_0 = 30$ kPa crossing the obstacle with OAR= 25%. Shocks propagate along the walls after reflection of the diffracted shock and interact in pairs at the four corners of the tube (Fig. 8, 2). This interaction produces four "hot spot" domains where over-compressed detonations ignite the gases pre-shocked by waves propagating along the adjacent walls (Fig. 8, 3-4). The resulting detonation catches up with the waves reflected downstream of the obstacle, propagates into the fresh mixture, and re-stabilizes such as before the obstacle (Fig. 8, 5). Soot recordings show the symmetry of the phenomenon on one of the tube walls. Smaller cells than upstream of the obstacle indicate the overdriven detonation.

These two mechanisms of re-initiation by shock-shock interaction (at the corner and the center of the square tube) can both occur during the same experiment, as in Figure 9, where the detonation initiated at the corner quenches before re-initiation by the convergence of the shocks on the centerline of the tube.

Re-initiations by shock-shock interaction were never observed in the round tube in our conditions.

3.3 Shock-wall Interaction Critical Scenarios

Figures 10 left, and 11 top, show chemiluminescence for $2\,H_2 + O_2$ at $p_0 = 30$ kPa and wall soot recordings for $2\,H_2 + O_2 + 2\,Ar$ at $p_0 = 50$ kPa downstream of the obstacle in the round tube. Figure 12 top shows soot recording for $2\,H_2 + O_2$ at $p_0 = 70$ kPa across the obstacle with OAR= 25% in the square channel.

In both the round tube and square channel, wall(s) are sites of hot spot ignition. The resulting flame is slow compared to the preceding shock(s), so they are not coupled. The deflagration propagates towards the end wall of the tube and partly around the walls, producing conical soot traces, that is, dark triangular regions typical of deflagration regimes. In the round tube, the flame self-accelerates and eventually undergoes Deflagration-to-Detonation Transition (DDT). When the transition occurs, a bright spot is visible on camera, and an overdriven detonation propagates on the entire cross-section. Repeated experiments in the round tube with the same mixture and initial conditions systematically showed DDT on the walls, but the

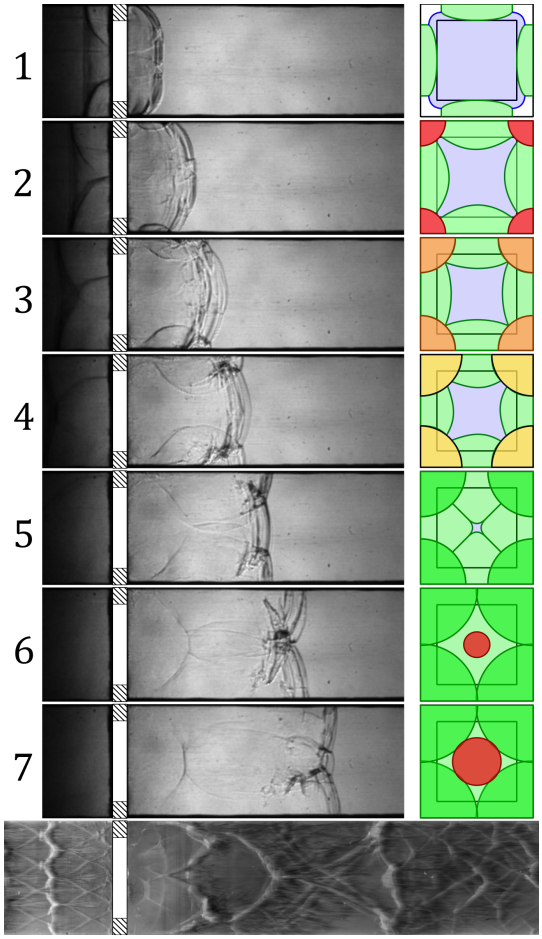

Fig. 9: Diffraction with OAR=50%. The mixture is $2\,H_2 + O_2 + 2\,Ar$ at $p_0 = 15$ kPa. Shadowgraph images (1 to 7, left: longitudinal recordings), parietal soot recording (bottom), front view schemes (right). $\Delta t_{\text{images}} = 6,0\ \mu$s.

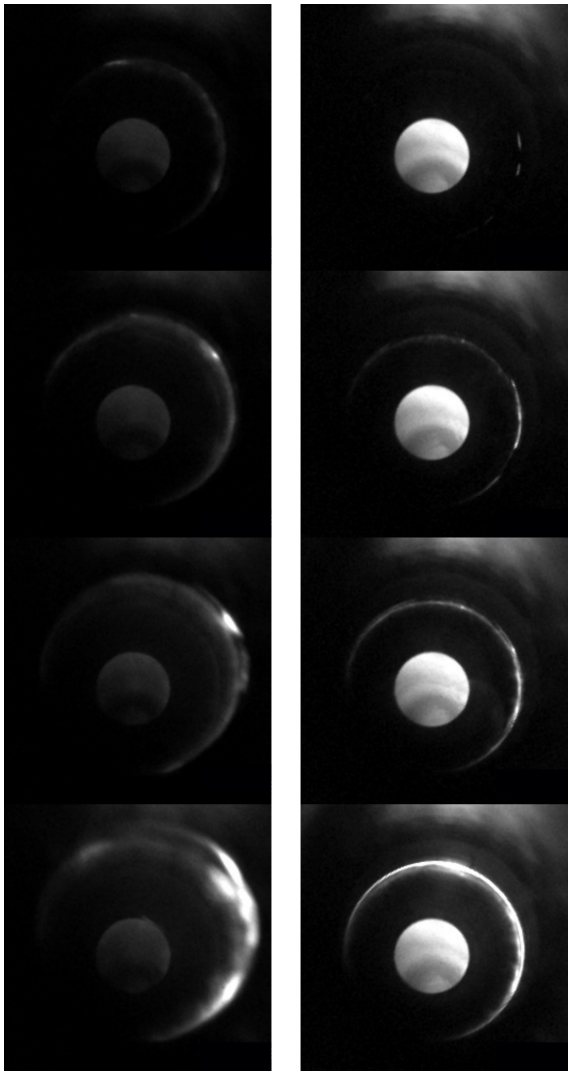

Fig. 10: Chemiluminescence imaging downstream of the obstacle in the round tube with OAR=25%. The mixture is $2\,H_2 + O_2$. Left: $p_0 = 30$ kPa, camera frequency is 15.5 kHz. Right: $p_0 = 80$ kPa, camera frequency is 125 kHz. The camera is slightly off-axis of the tube.

Kelvin-Helmoltz (KH) and Rayleigh-Taylor (RT) instabilities involved in DDT phenomena lead to poor repeatability regarding the hot spots number, azimuth angle position, distance from the obstacle and DDT run-up distances. The initiation of the detonation appears instantaneous compared to that of the deflagration. In the square tube, the deflagration ignition occurs in the center of a wall before being caught up by a re-ignited detonation in the corners. This deflagration is barely visible on shadowgraph images as the pressure gradients are small compared to that of the shock waves and burnt gases so soot recordings are needed to assess its occurring.

Figures 10 right, and 11 bottom, show chemiluminescence for $2\,H_2 + O_2$ at $p_0 = 80$ kPa and wall soot recordings for $2\,H_2 + O_2 + 2\,Ar$ at $p_0 = 60$ kPa downstream of the obstacle in the round tube. Figures 13, and 12 bottom, show the case of a detonation of $2\,H_2 + O_2 + 2\,Ar$ at $p_0 = 70$ kPa crossing the obstacle with OAR= 25% and soot recordings soot recording for $2\,H_2 + O_2 + 2\,Ar$ at $p_0 = 80$ kPa across the obstacle with OAR= 10% in the square channel. The reflected shock waves are strong enough to initiate an overdriven detonation. These

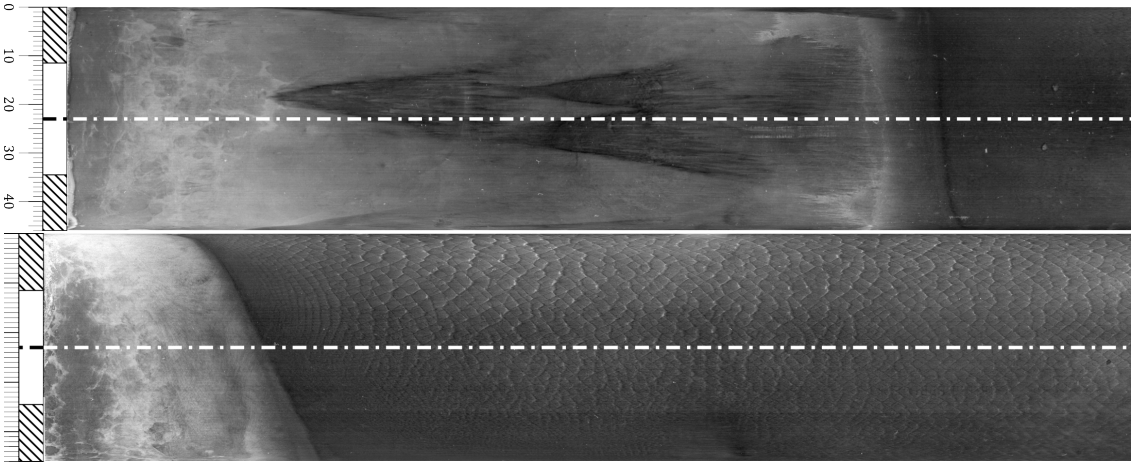

Fig. 11: Soot recordings from the downstream of the obstacle with OAR=25% in the round tube. The mixture is $2\,H_2 + O_2 + 2\,Ar$. Top: re-initiation by shock-wall reflection at $p_0 = 50$ kPa. Bottom: re-initiation by DDT at $p_0 = 60$ kPa.

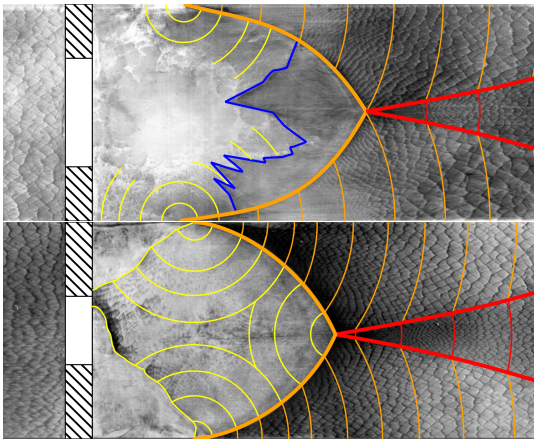

Fig. 12: Soot recordings of re-initiation by shock interaction in the corners of the square tube. Top: $2\,H_2 + O_2$, $p_0 = 70$ kPa, OAR= 25%, deflagration in center of wall. Bottom: $2\,H_2 + O_2 + 2\,Ar$, $p_0 = 80$ kPa, OAR= 10%, no deflagration. Yellow: highly overcompressed detonation, cells are barely visible. Orange: overcompressed detonation, growing cells. Red: overcompressed detonation. Blue: deflagration.

detonations recombine to form a self-sustaining detonation similar to the one upstream of the obstacle. In the round tube, the diffracted shock wave is reflected off the walls, creating a toroidal detonation initiation, as in figures 11 top, and 10 on the right. In practice, the soot foil placed around the wall made the cross-section shape slightly drop-shaped instead of round. The diffracted shock therefore reflected first on a point of the foil instead of a line, hence the non-axisymmetric recording.

3.4 Supercritical Scenario

Figure 14 shows the case of a detonation in $2\,H_2 + O_2$ at $p_0 = 50$ kPa crossing the opening obstacle with OAR= 75%. The decoupling between the combustion shock waves is not sufficient when the diffracted shock wave is reflected at the tube walls. Cells downstream of the obstacle may be larger than cells upstream before re-stabilizing to their initial width.

From $p_0 = 7.5$ to 50 kPa, the detonation is transmitted in the round and square tubes for the obstacle with OAR= 75%.

4 Discussion and conclusions

This work is an analysis of the three-dimensional transients that follow the diffraction of a steady cellular detonation through a single-hole obstacle in straight tubes. The focus is on the influence of the cross-sectional shape of the tube, namely round or square. The work extend our previous study on this influence on the cellular structure of a steadily-propagating detonation [29, 4]. We have identified 6 diffraction scenarios, comprising 1 subcritical, 4 critical and 1 supercritical behaviors.

Figure 15 summarizes these scenarios with OAR below or equal to 50% studied, as only supercritical

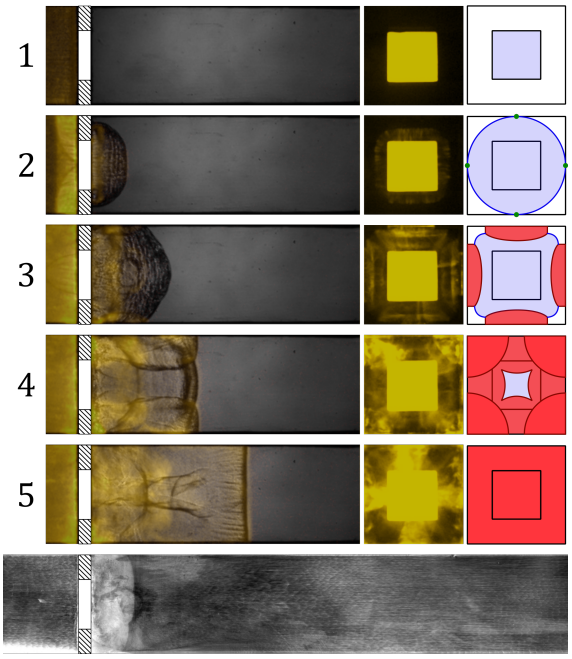

Fig. 13: Diffraction with OAR=25%. The mixture is $2\,H_2 + O_2 + 2\,Ar$ at $p_0 = 70$ kPa. Superposition of colorized chemiluminescence and shadowgraph images (1 to 5, left: longitudinal recordings), chemiluminescence front recordings (middle), parietal soot recording (bottom), and front view schemes (right). $\Delta t_{\text{images}} = 4$ μs.

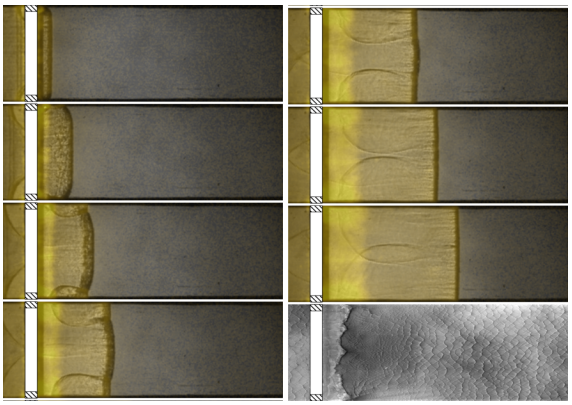

Fig. 14: Superposition of colorized chemiluminescence and shadowgraph images and soot recording of a detonation after diffraction passing through the obstacle with OAR= 75%. The mixture is $2\,H_2 + O_2$ at $p_0 = 50$ kPa. $\Delta t_{\text{images}} = 3$ μs.

behaviors are observed at OAR = 75%. No re-ignition by shock refocusing occurred in the round tube. Only extinction without re-ignition, DDT, re-ignition by wall-shock interaction, and transmission scenarios occurred, as already reported [32]. This is due to the concentricity of the tube and the diffracted shock. The latter reflects along a line, *i.e.*, the perimeter of the section, and not at one or more points. This systematically produces a more powerful toroidal reflected shock wave than in the square tube. On the other hand, the absence of corners in the round tube limits the promoting effects of turbulence and hot spots caused by friction at the walls.

A different scenario can occur in the square and round tubes with all other parameters identical, *i.e.*, with the same OAR, mixture, and p_0, for obstacles with open area ratios OAR= 10, 25, and 50%. A first explanation would be to invoke the difference in cell width $\bar{\lambda}$ from one tube to the other over the pressure range $p_0 \leq 30$ kPa. However, for OAR= 10%, the observed scenario differs from one cross-sectional shape to the other, despite the negligible influence of this shape for steady propagation of detonation [29]. The tube cross-section shape influences transient phenomena on a wider range of initial pressures than quasi-steady propagation. The criteria on the number $\mathcal{O}(100)$ of self-confined cells, *i.e.*, for confinement geometry that no longer affect the detonation dynamics, does not stand for transient phenomena. Thus, for $2\,H_2 + O_2 + 2\,Ar$ at $p_0 = 80$ kPa, re-ignition occurs by DDT in the round tube and by shock-shock interaction in the square tube. In addition, figure 15 shows the observed scenarios as a function of tube, mixture, OAR, and cell width upstream of the obstacle $\bar{\lambda}$ or the hydraulic diameter of the aperture to cell mean width ratio $d_h/\bar{\lambda}$.

For an equivalent cell size, with OAR= 25% and $2\,H_2 + O_2$, or with OAR= 10% and $2\,H_2 + O_2 + 2\,Ar$, the extinction conditions without re-ignition are the same, but such comparison does not stand for other (mixture, OAR) couples. Overall, the range of cell widths for re-ignition is higher in square than round tubes. The subcritical scenario has a wider limits, *i.e.*, occurs up to higher p_0, when detonating a more unstable mixture, as reported by [24].

Under our conditions, we cannot identify any criterion using the aperture-to-cell widths ratio as for diffraction in unconfined volumes [39], nor the distance between the closest wall and the aperture as

in the 2D phenomena studied by [35], that guarantees re-ignition. Our choice was to compare tubes of equal cross-section areas, but results show that the re-initiations by shocks downstream of the obstacle are a function of their strength, therefore with an implication of distances from the obstacle rather than surfaces. DDT occurs at walls within boundary layers, hence comparison between tubes should also involve equal parietal surfaces of the confinement rather than equal cross-sectional surfaces, with special attention on interacting boundary layers, *e.g.*, in channels with small aspect ratios or at corners. The cell size alone can not be used for predicting transients in three-dimensional configurations.

Our observations lead to a discussion of dimensionality for transient detonation dynamics. In the round tube, the phenomena are 2D axisymmetric, except for the DDT scenario where wall surface is involved. In the square tube, diffraction through a square hole can induce 2 pairs of opposing fronts originating independently of each other from the opposite walls (Fig. 13), or 4 fronts originating from the corners, depending on the interaction of adjacent shocks (Fig. 8). The first case is as a pair of 2D re-initiations, but the latter is 3D, and would not have occurred if the hole in the obstacle was a slit. Therefore, some care should be taken when classifying experimental channels as two- or three-dimensional depending on their aspect ratio. Even wide tubes can be considered as two-dimensional for global transient phenomena if their configuration can be seen as an extrusion of a two-dimensional configuration, regardless of length, *e.g.*, a backward-facing step [40], or a perforated plate with a distribution and density of holes that makes the transverse directions indistinguishable from each other [28]. This study suggests that the simple configurations necessary for laboratory experiments to more easily identify fundamental phenomena cannot always be used to anticipate the transients that would occur in industrial configurations.

Availability of data and materials and supplementary material

The data that support the conclusions of this study are available from the corresponding author upon reasonable request. The shadowgraph and chemiluminescence video recordings will be provided as supplementary material.

Acknowledgements

This work was supported by the Ministry of Higher Education, Research and Innovation (France) and the CPER-FEDER Project of *Région Nouvelle Aquitaine*.

References

[1] J. X. Wen, E. S. Hecht, R. Mevel, Recent advances in combustion science related to hydrogen safety, Progress in Energy and Combustion Science 107 (2025) 101202. doi:https://doi.org/10.1016/j.pecs.2024.101202.

[2] Y. Liu, J. Lee, R. Knystautas, Effect of geometry on the transmission of detonation through an orifice, Combustion and Flame 56 (2) (1984) 215–225. doi:https://doi.org/10.1016/0010-2180(84)90038-5.

[3] V. Monnier, Aspects tridimensionnels de la détonation cellulaire : des observations expérimentales et un modèle (in french), Ph.D. thesis, École Nationale Supérieure de Mécanique et d'Aérotechnique (2023). doi:https://doi.org/10.13140/RG.2.2.17111.85921.

[4] V. Monnier, V. Rodriguez, P. Vidal, R. Zitoun, Three-dimensional dynamics of detonation diffraction: effects of the tube cross-section shape, Proc. 29$^{\text{th}}$ ICDERS, Paper 59.

[5] S. Ohyagi, T. Obara, S. Hoshi, P. Cai, T. Yoshihashi, Diffraction and re-initiation of detonations behind a backward-facing step, Shock Waves 12 (2002) 221–226. doi:https://doi.org/10.1007/s00193-002-0156-z.

[6] J. Klein, O. Samimi-Abianeh, Simultaneous schlieren and direct photography of detonation diffraction regimes in hydrogen mixtures, Combustion and Flame 272 (2025) 113845. doi:https://doi.org/10.1016/j.combustflame.2024.113845.

[7] R. Bhattacharjee, S. Lau-Chapdelaine, G. Maines, L. Maley, M. Radulescu, Detonation re-initiation mechanism following the mach reflection of a quenched detonation, Proceedings of the Combustion Institute

34 (2) (2013) 1893–1901. doi:https://doi.org/10.1016/j.proci.2012.07.063.

[8] X. Shi, J. Pan, C. Jiang, J. Li, Y. Zhu, E. K. Quaye, Effect of obstacles on the detonation diffraction and subsequent re-initiation, International Journal of Hydrogen Energy 47 (10) (2022) 6936–6954. doi:https://doi.org/10.1016/j.ijhydene.2021.12.026.

[9] P. Vieille, Rôle des discontinuités dans la propagation des phénomènes explosifs, Comptes Rendus de l'Académie des Sciences (1900) 413–416.

[10] Y. Zeldovich, G. Barenblatt, Theory of flame propagation, Combustion and Flame 3 (1959) 61–74. doi:https://doi.org/10.1016/0010-2180(59)90007-0.

[11] F. Pintgen, J. Shepherd, Detonation diffraction in gases, Combustion and Flame 156 (3) (2009) 665–677. doi:https://doi.org/10.1016/j.combustflame.2008.09.008.

[12] M. Arienti, J. Shepherd, A numerical study of detonation diffraction, Journal of Fluid Mechanics 529 (2005) 117–146. doi:https://doi.org/10.1017/S0022112005003319.

[13] R. Soloukhin, K. Ragland, Ignition processes in expanding detonations, Combustion and Flame 13 (3) (1969) 295–302. doi:https://doi.org/10.1016/0010-2180(69)90007-8.

[14] D. H. Edwards, G. O. Thomas, M. A. Nettleton, The diffraction of a planar detonation wave at an abrupt area change, Journal of Fluid Mechanics 95 (1) (1979) 79–96. doi:https://doi.org/10.1017/S002211207900135X.

[15] D. Edwards, G. Thomas, M. Nettleton, Diffraction of a planar detonation in various fuel-oxygen mixtures at an area change, AIAA Progress In Astro. and Aero. (1979) 341–357.

[16] R. Knystautas, J. Lee, C. Guirao, The critical tube diameter for detonation failure in hydrocarbon-air mixtures, Combustion and Flame 48 (1982) 63–83. doi:https://doi.org/10.1016/0010-2180(82)90116-X.

[17] Y. B. Zeldovich, S. Kogarko, N. Simonov, An experimental investigation of spherical detonation in gases, Soviet Phys. tech. Phys. 1 (1689) (1956) 1689.

[18] G. Ciccarelli, S. Dorofeev, Flame acceleration and transition to detonation in ducts, Progress in Energy and Combustion Science 34 (4) (2008) 499–550. doi:https://doi.org/10.1016/j.pecs.2007.11.002.

[19] J. Lee, R. Knystautas, N. Yoshikawa, Photochemical initiation of gaseous detonations, Acta Astronautica 5 (11) (1978) 971–982. doi:https://doi.org/10.1016/0094-5765(78)90003-6.

[20] N. Yoshikawa, Coherent shock wave amplification in photochemical initiation of gaseous detonations, Ph.D. thesis, McGill University (1978).

[21] A. A. Vasil'ev, Cell size as the main geometric parameter of a multifront detonation wave, J. of Propulsion and Power 22.

[22] V. Mitrovanov, R. Soloukhin, The diffraction of multifront detonation waves, Sov. Phys. Dokl. 9 (1964) 1055–1058.

[23] I. O. Moen, G. O. Thomas, D. Bjerketvedt, P. A. Thibault, Influence of cellular regularity on the behavior of gaseous detonations, in: Dynamics of Explosions, Vol. 104, Progress in Astronautics and Aeronautics, 1986, Ch. III. Detonation Structure and Limit Propagation, pp. 220–243. doi:https://doi.org/10.2514/5.9781600865800.0220.0243.

[24] M. Kuznetsov, V. Alekseev, S. Dorofeev, Comparison of critical conditions for ddt in regular and irregular cellular detonation systems, Shock Waves 10 (2000) 217–223. doi:https://doi.org/10.1007/s001930050009.

[25] S. Dorofeev, V. Sidorov, M. Kuznetsov, I. Matsukov, V. Alekseev, Effect of scale on the onset of detonations, Shock Waves 10 (2000) 137–149. doi:https://doi.org/10.1007/s001930050187.

[26] M. J. Plaster, R. McClenagan, F. J. Benz, J. E. Shepherd, J. H. S. Lee, Detonation of cryogenic gaseous hydrogen-oxygen mixtures, Progress in Astronautics and Aeronautics 133 (1991) 37–55.

[27] C. Guirao, R. Knystautas, J. Lee, W. Benedick, M. Berman, Hydrogen-air detonations, Symposium (International) on Combustion 19 (1) (1982) 583–590, nineteenth Symposium (International) on Combustion. doi:https://doi.org/10.1016/S0082-0784(82)80232-4.

[28] V. Rodriguez, V. Monnier, P. Vidal, R. Zitoun, Non-dimensionalized distances and limits for the transition of deflagration to detonation, Shock Waves 32 (2022) 417–425. doi:https:

//doi.org/10.1007/s00193-022-01088-0.

[29] V. Monnier, V. Rodriguez, P. Vidal, R. Zitoun, An analysis of three-dimensional patterns of experimental detonation cells, Combustion and Flame 245 (2022) 112310. doi:https://doi.org/10.1016/j.combustflame.2022.112310.

[30] V. Monnier, V. Rodriguez, P. Vidal, R. Zitoun, Three-dimensional dynamics of detonation cells in linearly diverging channels: experimental analysis of the cross-sectional shape and a detonation-shock dynamics interpretation, Exp. Fluids 65 (2024) 154. doi:https://doi.org/10.1007/s00348-024-03893-y.

[31] S. Boulal, Comportements dynamiques de la détonation dans les écoulements des compositions gazeuses non-uniformes, Ph.D. thesis, École Nationale Supérieure de Mécanique et d'Aérotechnique (2017).

[32] G. Ciccarelli, J. Boccio, Detonation wave propagation through a single orifice plate in a circular tube, Symposium (International) on Combustion 27 (2) (1998) 2233–2239. doi:https://doi.org/10.1016/S0082-0784(98)80072-6.

[33] A. A. Vasil'ev, Diffraction of multifront detonation, Combustion, Explosion and Shock Waves 24 (1988) 92–99. doi:https://doi.org/10.1007/s00193-012-0409-4.

[34] E. Pantow, M. Fischer, T. Kratzel, Decoupling and recoupling of detonation waves associated with sudden expansion, Shock Waves 6 (1996) 131–137. doi:https://doi.org/10.1007/BF02510993.

[35] H. Sun, A. Kawasaki, N. Itouyama, K. Matsuoka, J. Kasahara, Experimental study on detonation-diffraction reflection point distances in hydrogen and gaseous hydrocarbon reactive systems, Combustion and Flame 245 (2022) 112329. doi:https://doi.org/10.1016/j.combustflame.2022.112329.

[36] R. Sorin, R. Zitoun, B. Khasainov, D. Desbordes, Detonation diffraction through different geometries, Shock Waves 19 (2009) 11–23. doi:https://doi.org/10.1007/s00193-008-0179-1.

[37] N. L. Polley, M. Q. Egbert, E. L. Petersen, Methods of re-initiation and critical conditions for a planar detonation transforming to a cylindrical detonation within a confined volume, Combustion and Flame 160 (1) (2013) 212–221. doi:https://doi.org/10.1016/j.combustflame.2012.09.017.

[38] V. Yousefi-Asli, S. Lau-Chapdelaine, G. Ciccarelli, Novel weak detonation initiation from normal shock reflection in square cross-section shock tubes, Combustion and Flame 266 (2024) 113502. doi:https://doi.org/10.1016/j.combustflame.2024.113502.

[39] O. Peraldi, R. Knystautas, J. Lee, Criteria for transition to detonation in tubes, Symposium (International) on Combustion 21 (1) (1988) 1629–1637, twenty-First Symposuim (International on Combustion). doi:https://doi.org/10.1016/S0082-0784(88)80396-5.

[40] Y. Poroshyna, J. Loiseau, S. S.-M. Lau-Chapdelaine, G. Ciccarelli, 3d effects of detonation re-initiation after diffraction at a back-facing step, Proceedings of the Combustion Institute 40 (1) (2024) 105325. doi:https://doi.org/10.1016/j.proci.2024.105325.

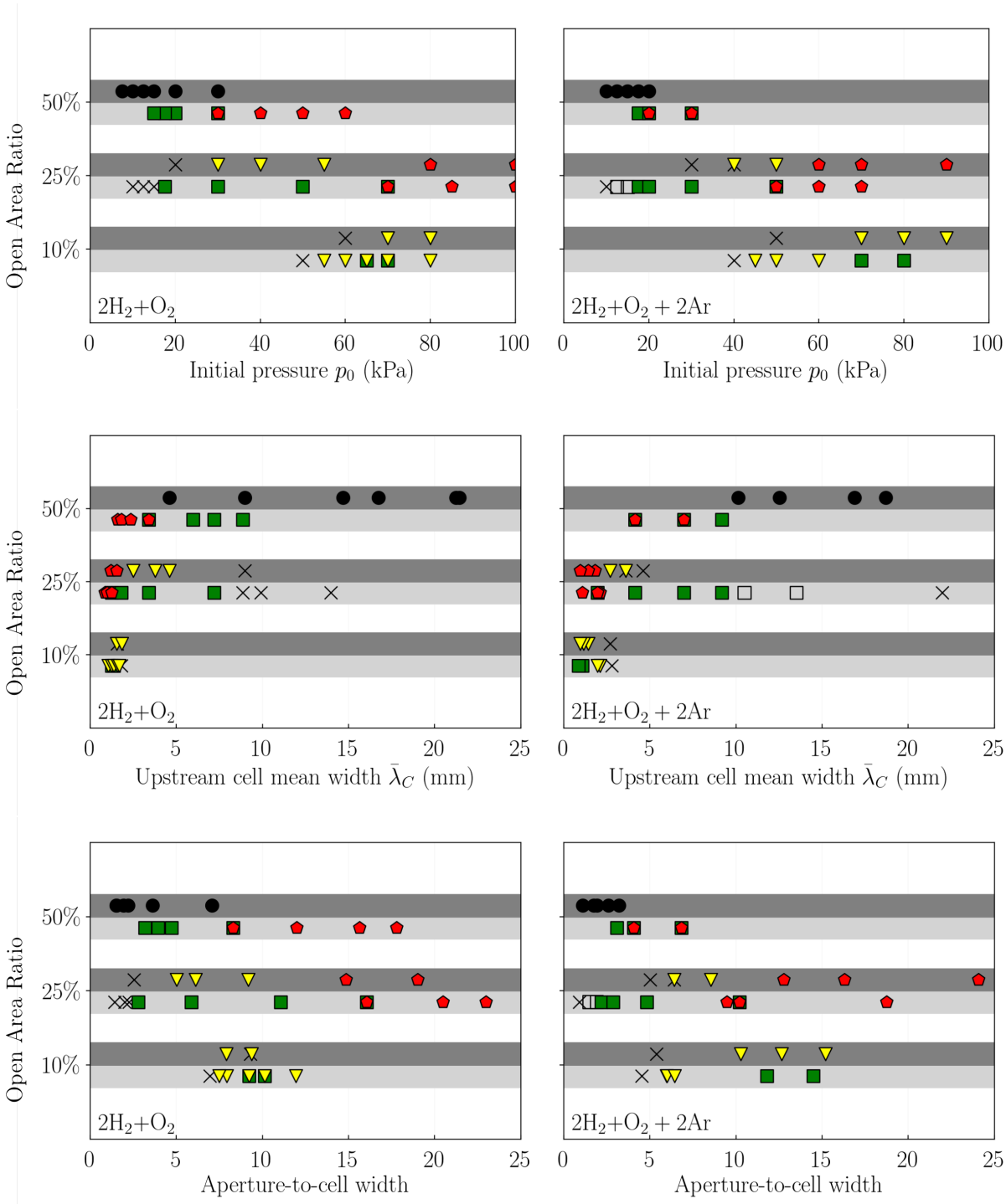

Fig. 15: Scenarios based on OAR and tube cross-section (dark grey: round, light grey: square). (×) no re-ignition, (□) re-ignition by tube-center shock interaction, (■) re-ignition by corner-shock interaction, (⬟) re-ignition by wall-shock interaction, (▽) re-ignition by TDD, (●) transmission.